Vol. 08, No. 3 (2026) 1551-1570, doi: 10.24874/PES08.03.013

Proceedings on Engineering Sciences

www.pesjournal.net

ADVANCED FREQUENCY CONTROL IN MICROGRID-CONNECTED HYBRID POWER SYSTEMS VIA SMES-BASED NEURAL NETWORK CONTROLLER OPTIMIZED WITH SINE COSINE ALGORITHM

M. Mujtahid Ansari[1]
Prashant J. Gaidhane

Received 02.06.2026.
Revised 28.07.2026.
Accepted 26.08.2026.

Keywords:

Diesel-engine generator, Neural network, Photovoltaic, Sine cosine optimization, Superconducting magnetic energy storage

A B S T R A C T

This paper focuses on frequency regulation in a microgrid connected hybrid power system incorporating renewable energy sources i.e. solar PV generation and wind power generation, diesel engine generator (DEG) and superconducting magnetic energy storage (SMES) unit. Renewable intermittency and uncontrolled load change causes large frequency deviation and requires fast and adaptive control supports. In order to overcome this issue, Sine Cosine Optimized Neural Network Controller (SCONN) is proposed for dynamic SMES power modulation and DEG is used for sustained secondary frequency regulation. The proposed controller parameters are optimized by the Sine Cosine Optimization algorithm to provide better damping and less during transient oscillations and under different operating conditions. MATLAB/Simulink simulations are performed in the case of step and continuous load disturbance. Results show that with the SCONN controller the maximum frequency deviation is mitigated down to 0.189 Hz from 0.323 Hz (PID) with 62.1% reduction in ITSE as well as with 39.7% reduction in overshoot. Compared to the PI controller the maximum deviation improvement is 54.8%. The obtained responses confirm that a SMES sustained by SCONN control helps to significantly increase frequency stability in hybrid microgrid function.

© 2026 Published by Faculty of Engineering

1. INTRODUCTION

With the shift towards sustainable energy solutions, the widespread use of renewable energy sources has been integrated into modern power systems where microgrid integrated hybrid power systems have emerged. However, these systems combining Solar PV, wind energy and Diesel Engine Generators (DEG), present an effective and sustainable way to address the growing need for dependable electrical supply. Nevertheless, lack of stability and operational efficiency is greatly challenged by the inherent intermittency of the renewable

Corresponding author: M. Mujtahid Ansari
Email: mujtahidansari@gmail.com

sources and the unpredictability of the load variations (Belboul et al., 2022).

Frequency instability, which is caused by frequent changes of demand load and unpredictable fluctuations of renewable power generation is a major issue for hybrid power systems. However, such variations can render microgrid connected systems difficult to maintain a continuous and stable operation and necessitate the introduction of advanced frequency regulation mechanism. Given the importance of addressing this challenge to enable the long-term feasibility of hybrid power systems and to support the growth of resilient and environmentally sustainable energy infrastructure, greater efforts are necessary to improve the performance of this key component in hybrid power systems.

Thus, this study addresses the critical role of Superconducting Magnetic Energy Storage (SMES) in overcoming frequency fluctuations of various microgrid connected hybrid power systems (Khaleel et al., 2023). The SMES technology that is characterized by its fast response and low energy loss during charge and discharge cycles is a promising solution to enhance frequency stability. However, the application of SMES in frequency regulation is considerably influenced by its control strategy efficiency. This research introduces a controller that is a Neural Network (Abdolrasol et al., 2021) based, with fine-tuned using the Sine Cosine Optimization (SCO) algorithm (Hassan et al., 2024) that optimizes its performance. The adopted hybrid controller uses the ability of neural networks to provide adaptability to dynamic system response in combination with SCO to enhance system parameter selection, which endows the regulator with precise and robust frequency regulation.

The structure of the study is based on two phases of simulations to fully account for the effect of SMES on frequency stability under various operating conditions. The system is first analyzed in the first phase with Proportional Integral (PI) controller, to determine the system stability and system response to sudden load changes. The second phase applies the analysis to a typical operational period, considering the system's ability to work under real time variations of load demand. A framework has been developed for a dual phase simulation of SMES performance that not only provides an understanding of SMES performance in both stable and variable environments but also information about possible hardware improvements.

To further refine the controller performance, the research incorporates optimized inductor current constraints, which avoid discontinuous conduction and storage constraints which may hinder system efficiency. Using a hybrid optimization strategy for the controller tuning, the study shows the best way to make a balance between responsiveness and stability to finally achieve robust controller for frequency regulation in hybrid power systems.

The purpose of this research is to develop effective frequency control mechanisms for microgrid-connected hybrid power systems. The study, which emphasizes the critical role of SMES, demonstrates through advanced neural network-based control strategy optimized through Sine Cosine Optimization, can help in the improvement of system stability when power generation is fluctuating and load demand is equally unpredictable. The results could impact future robustness of the power infrastructure designs in forming smart, intelligent and resilient power management systems.

The contributions of this work are as follows:

- It is suggested to use a Sine Cosine Optimized Neural Network (SCONN) controller to real-time optimize SMES power modulation, which, as far as we know, has not been implemented previously to regulate the frequency in a hybrid power system linked to the microgrids.
- In comparison to the traditional PI/PID controllers, the proposed technique employs a three-layer neural network with the offline-trained weights that can adapt the control and provide non-linear control without retraining under the Sine Cosine Algorithm.
- The experiment clearly presents and imposes constraints on the SMES coil inductor current (maximum and minimum law) to prevent discontinuous conduction and storage saturation that has been widely ignored until now in other studies on frequency control using SMES.
- An overall two-stage simulation procedure (step perturbations and time-varying load/renewable profiles) is created, and a performance comparison table with current state-of-the-art approaches validates the advantage of the proposed SCONN controller.

The rest of this paper is organized as follows: A broad literature review of related works is presented in section 2. The proposed methodology and control strategy are laid out in Section 3. The results from the simulation are discussed in the fourth Section of this document and an analysis is presented to explain the mechanism of operation. Finally, Section 5 concludes with a summary of the main findings and a summary of the conclusion.

2. LITERATURE REVIEW

With the global attention directed toward clean and sustainable energy because of its growing impact of greenhouse gases on Earth’s atmosphere and the depletion of fossil fuels, energy alternatives are picking up speed. There are multiple renewable energy sources, of which hydro energy, solar energy, wind energy and biogas are main candidates for a cleaner and more environmentally friendly energy transition (Babatunde et al., 2020; Ullah et al., 2021). With a growing interest in exploiting wind and solar power to enlarge electricity generation role, there also has been an increasing focus

on the integration of wind and solar power into distributed generation systems and microgrids (Iweh et al., 2021). Despite the advantage of solar power supply to off grid area while grid extension is impractical, wind power is usually attributed to grid-based use. Solar photovoltaic (PV) systems are flexible, being easily installable at residence and commercial places that make them a good option for decentralized energy systems (Zisos et al., 2024).

In the deployment of wind and solar PV power plants for distributed generation and microgrids, variable power outputs of those sources are exploited in either meeting local power needs or provide excess electricity to the grid (Dawn et al., 2024). The intermittency and unpredictability of renewable energy sources however bring about a number of technical, economic and social issues (Sánchez et al., 2022). Technical issues arise from integrating these variable energy sources into existing grids and microgrids at the frequency and voltage stability levels. The uncertainty of distributed renewable energy sources requires a fast development for tackling the operation challenges to maintain stable and efficient grid operation.

Energy storage technologies thus support the mitigating of the frequency regulation challenges of microgrid connected hybrid power systems. In the literature, multiple functions have been proposed for the use of modern energy storage solutions like providing backup power supply, active and reactive power management as well as performing energy absorption or injection to the grid (Choudhury, 2022; Saxena & Shankar, 2022; Ullah et al., 2024). However, such traditional storage options such as BESS (Rana et al., 2021) and Hydro Pump Storage (Coban et al., 2022) suffer from their slow response times, small levelized cost of storage, storage capacity limitations, large spatial requirements, and possible environmental concerns (Adefarati et al., 2023, 2024).

This study proposes adopting the Superconducting Magnetic Energy Storage (SMES) technology to improve the stability of hybrid power systems to solve these challenges. The advantages of SMES are that it can respond rapidly, store efficiently, and inject or absorb real and reactive power as needed, making it a good solution for grid stability (Yadav and Saravanan, 2023; Jalilian et al., 2023). SMES has been studied previously in the context of mitigating transient disturbances in grid connected systems (Choudhury, 2022) and enables both on grid and off grid operation (Jalilian et al., 2023). In addition, many studies on neural network-based frequency control (Safari et al., 2021), power flow control and management strategies using energy storage systems (Chen & Chang, 2022), as well as power flow control algorithms based on knowledge-based approaches (Venkatesan & Govindarajan, 2019), have been conducted.

This paper provides some novel contributions which build upon prior research efforts. A series of frequency stability analysis of a microgrid connected hybrid power system with solar PV, wind, and Diesel Engine Generator (DEG) sources are also included. Frequency response of the system is enhanced through the implementation of a Neural Network based controller that is optimized for using the Sine Cosine Optimization (SCO) algorithm. Dynamic performance and stability under sudden changes in load demand and renewable power fluctuations have been improved through the optimization process that allows precise tuning of the controller parameters. Refined constraints on inductor current are also imposed to minimize discontinuous conduction and storage limitations of the Superconducting Magnetic Energy Storage (SMES) system. By filling significant disconnects in the present literature, these disparities make vital contributions to intelligent frequency regulation techniques and highlight the key functionality of SMES and sophisticated regulate with regards to microgrid balance.

Research Gap: Although there have been many studies on the integration of renewable energy sources into hybrid power systems, there are still several unresolved gaps. Up to now, much of the research in the literature has been concentrated on conventional methods of frequency regulation, and traditional energy storage systems, including Battery Energy Storage Systems (BESS) and Hydro Pump Storage; however, the benefits of Superconducting Magnetic Energy Storage (SMES) in the context of microgrid application needs to be explored further. Additionally, while many different optimization technologies have been utilized to tune the controller in the power management, there is limited research conducted on the application of the Sine Cosine Optimization (SCO) algorithm for the controller optimization using neural network-based controllers in hybrid power systems. Moreover, they lack studies on the effect of refined inductor current constraints in preventing discontinuous conduction in the SMES system. These gaps indicate the urgent need to develop the superior advanced intelligent control strategies that can contribute to the enhancement of the microgrid connected hybrid power systems' frequency stability and dynamic performance.

Findings from Literature: It is shown from the literature review that in terms of frequency and voltage stability, the integration of renewable energy sources into microgrids provide significant benefits, although several challenges remain. SMES has great potential to upgrade grid stability by virtue of their high efficiency and rapid response time. However, the interface between different frequency control and power management strategies has been explored in previous studies, but the utilization of hybrid optimization techniques for controller tuning has not. Additionally, the studies have largely been conducted in the transient condition, with little attention given to the employment of SMES in steady state

operating conditions. It highlights the need for the development of hybrid power systems stability by incorporating SMES into a full optimization methodology.

3. PROPOSED METHODOLOGY

Hybrid Power Systems (HPS) are integrated systems of more than one energy sources (Solar, wind, diesel generator etc.) and energy storage systems to have a long life and reliable energy. This section presents in detail the theoretical framework and also the mathematical modeling of the crucial parts of HPS including the solar photovoltaic (PV) systems, wind turbines and Diesel engine generators (DEG). It is the models that are based on the first principle of conservation of energy and system dynamics. The proposed block diagram in Figure 1 represents a micro-grid - connected Hybrid Power System (HPS) containing solar PV, wind turbine, diesel engine generator (DEG), energy storage system (ESS) and SMES system coordinated by an advanced Sine Cosine Optimized Neural Network (SCONN)-based control strategy. The PV subsystem and the wind subsystem correspond to the renewable power generation of the systems using MPPT controllers to draw maximum available power available and the DEG is responsible for a stable backup generation using a PID controlled governor engine loop. All power contributions are summed and compared against the load demand at the power balance junction resulting in a power mismatch signal causing system frequency deviation. This frequency deviation is modelled by the system inertia and damping characteristics and it is fed to both DEG-PID controller and SCONN controller. The SCONN controller dynamically regulates the SMES unit to inject or absorb power quickly, providing frequency support in a short time, while at the same time, optimising the DEG response to provide more or less effectiveness to sustained regulation. The combined effect of SMES (fast response) and DEG (secondary control) helps to minimise the frequency deviations and ensure effective frequency compensation under different load and renewable generation conditions. Overall, the proposed architecture increases the stability of the system, improves the dynamic performance, and facilitates the integration of renewable sources of energy into the hybrid system.

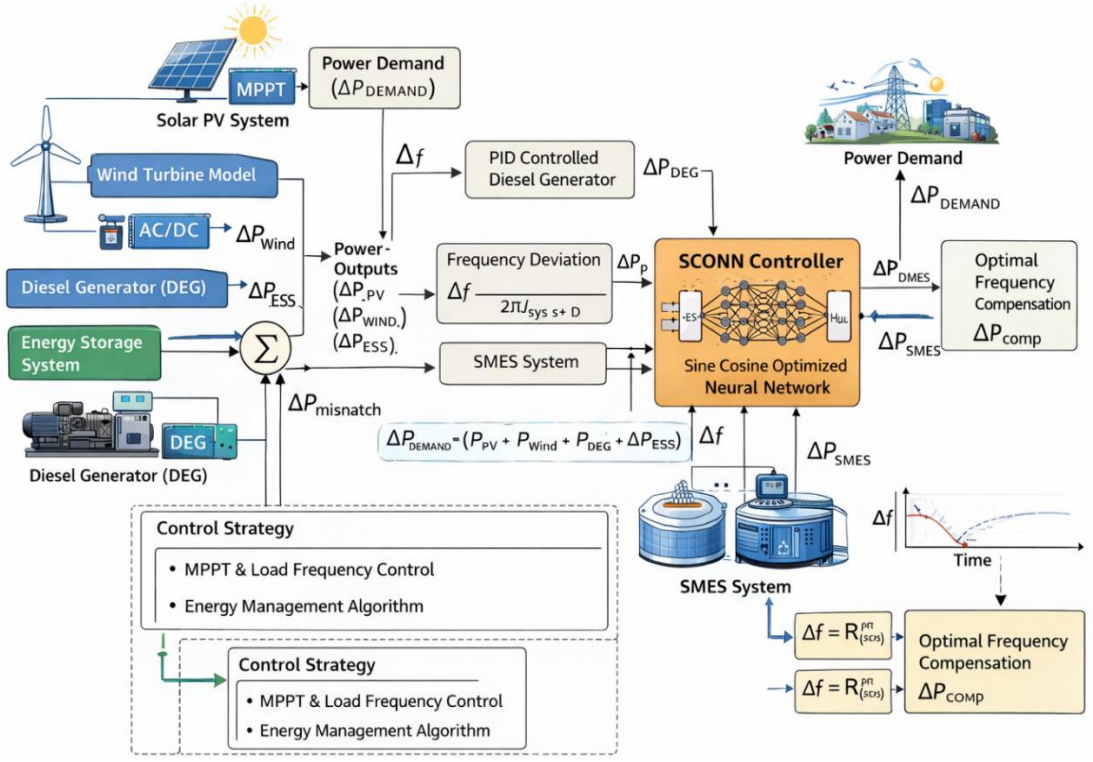


Figure 1. Block Diagram of Microgrid-Connected Hybrid Power System with SCONN-Based SMES Frequency Control

3.1 Solar Photovoltaic (PV) Model

The solar PV model is basically an electrical power output by solar panels dependent on incident solar irradiance and the physical properties of the PV cells. Factors like solar irradiance, cell efficiency, and temperature and other environmental based losses affect power output of a PV system.

3.1.1 Power Output Equation

The PV array delivers electrical power output (P_{PV}) according to the following formula:

$$P_{PV} = A \cdot \eta \cdot G \cdot PR \quad (1)$$

Where:

- The calculation requires surface area measurement of PV array devices (A) and efficiency value (η) and solar irradiance measurement (G) and performance ratio data (PR) to determine PV cell output current (I_{pv}).
- PV cell efficiency stands at η equal to percent efficiency while using the symbol %.
- The solar irradiance measurement stands at G (W/m²).
- Performance Ratio (PR) represents the performance measurement that deducts losses from shading and dirt as well as temperature impacts.

3.1.2 Ideal Solar Cell Equation

The I-V characteristic of a solar cell follows the ideal diode equation.

$$I_{PV} = I_L - I_0\left(e^{\frac{V_{PV}+I_{PV}\cdot R_S}{n\cdot V_t}} - 1\right) \qquad (2)$$

Where:

- The PV cell produces I_{pv} along its output as an output current which measures in amperes (A).
- The light-generated current I_L measures in amperes (A).
- The quantity I_0 refers to the reverse saturation current (A).
- V_{pv} stands as the voltage that develops across the PV cell while measuring in units of Volt (V).
- The series resistance of the cell equals R_s in units of Ω.
- The proper operational behavior of the diode depends on its ideality factor η which falls within 1 and 2.
- The thermal voltage V_t takes this expression $V_t = \frac{kT}{q}$ with Boltzmann's constant k and Kelvin temperature T and the electron charge q.

3.1.3 Equivalent Circuit Model for PV Modules

A PV module made up of serially and connected in parallel cells requires use of additional shunt resistance (R_{SH}) to adjust its current-voltage relationship:

$$I_{PV} = I_{SC} - I_{PH}\left(e^{\frac{V_{PV}+I_{PV}\cdot R_S}{n\cdot V_t}} - 1\right) - \frac{V_{PV} + I_{PV}\cdot R_S}{R_{SH}} \qquad (3)$$

Where:

- I_{SC} is the short-circuit current (A),
- I_{PH} is the photocurrent (A),
- R_{SH} is the shunt resistance (Ω).

3.1.4 Temperature Effects

As temperature rises, the efficiency of PV cells decreases. The power output function of PV cells depends on temperature as follows:

$$P_{PV}(T) = P_{PV}(T_{STC}).\left(1 - \beta.(T - T_{STC})\right) \qquad (4)$$

Where:

- The symbol $P_{PV}(T_{STC})$ represents power output at the standard test conditions (STC) standard.
- In the formula the temperature coefficient of power expressed as percent per degree Celsius appears as β.
- The operating temperature is specified by T which uses degrees Celsius units.
- The T_{STC} variable indicates the temperature measurement point which usually maintains STC at 25°C.
-

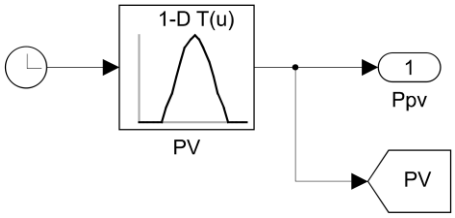


Figure 2. Modeling of Solar Photovoltaic (PV) Model

Figure 2 is the Simulink model of solar photovoltaic (PV) system that uses a 1-D look up table to calculate PV power output with observed irradiance and temperature.

3.2 Wind Speed to Power Conversion Model

The model is used to estimate the electrical power production of a wind turbine based on the aerodynamic principles, taking into account the influence of the changing wind speed, the density of the air, and the design of the wind turbine. The wind speed to power conversion model indicated in the Figure 3 describes the process of how the available kinetic energy in wind is converted to electrical power using a wind turbine. The model starts with the input of wind speed at hub height which is the free stream wind velocity. Due to aerodynamic interaction of rotor and incoming air flow, effective wind speed at the rotor is lowered by the axial induction factor and this represents the energy extraction from wind. The aerodynamic power intercepted by the turbine rotor is determined by using the basic wind power equation whose terms are air density, the rotor swept area, the cube of the wind speed and the power coefficient.

The power coefficient is a nonlinear function of the tip-speed ratio and rolling angle of the blade, which is the aerodynamic efficiency of the turbine under different working conditions. The four power factors are tip-speed ratio (angular speed of the rotor and the radius of the blades with the wind speed) and the pitch angle controls

the power capture with the high wind speed. Finally, the mechanical power out of the wind is converted to electric power with the generator and power electronics, as an efficiency factor. This comprehensive model effectively describes the aerodynamic properties, as well as the operational characteristics of wind turbines, which is appropriate for the dynamic and steady state analysis of hybrid power systems.

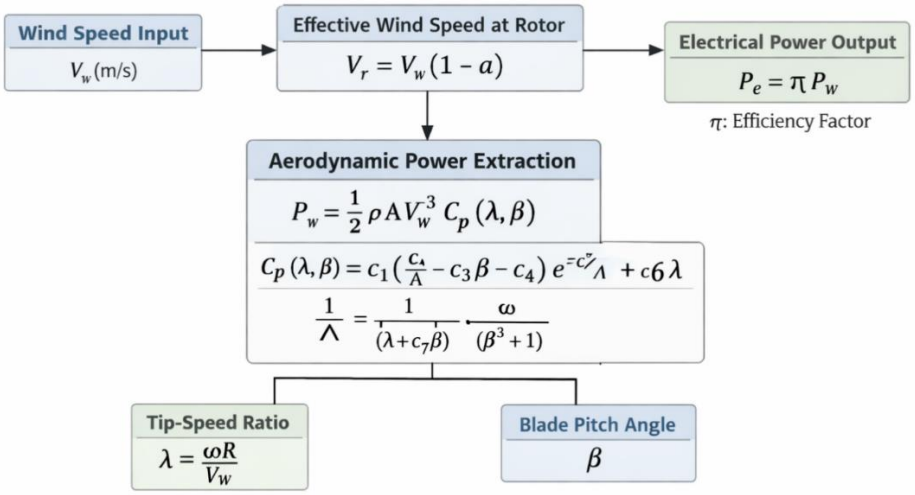


Figure 3. Wind Speed to Electrical Power Conversion Model of Wind Turbine

3.2.1 Aerodynamic Power Extraction

The fundamental mechanical power P_w that is collected by the rotor from the wind is given by:

$$P_w = \frac{1}{2}\rho A V_w^3 C_p(\lambda,\beta) \quad (5)$$

Where:

- ρ is the air density (kg/m^3),
- $A = \pi R^2$ is the swept area of the rotor (m^2),
- R is the rotor radius (m),
- V_w is the upstream wind speed undisturbed by the rotor (m/s),
- C_p is the power coefficient, representing the turbine's aerodynamic efficiency.

3.2.2 Effective Wind Speed at the Rotor (V_r)

The wind speed which is felt by the rotor (V_r) is lowered from the free-stream speed (V_w) due to the pressure field produced by energy extraction (actuator disc theory). A more accurate representation goes as follows:

$$V_r = V_w(1-a) \quad (6)$$

Where a is the axial induction factor. However, for system level modelling in which V_w is considered at the hub height, we often use V_w in Eq. (5) with a C_p curve that has the effect of accounting for this loss included in the curve.

3.2.3 Power Coefficient (C_p) Model

The power coefficient is a function of two parameters, the tip-speed ratio (λ) and the blade pitch angle (β). An empirical approximation which is commonly used is:

$$C_p(\lambda,\beta) = c_1\left(\frac{c_2}{\Lambda} - c_3\beta - c_4\right)e^{-\frac{c_5}{\Lambda}} + c_6\lambda \quad (7)$$

$$\text{with } \frac{1}{\Lambda} = \frac{1}{\lambda+c_7\beta} - \frac{c_8}{\beta^3+1} \quad (8)$$

Where:

- Tip-speed ratio: $\lambda = \frac{\omega R}{V_w}$ (dimensionless),
- ω is the rotor angular velocity (rad/s),
- c_1 to c_8 are empirical constants specific to the turbine design.

This form is a better model of the variation in C_p for various operating conditions.

3.3 Diesel Engine Generator (DEG) Model

The Diesel Engine Generator (DEG) model shown in the Figure 4 depicts both the steady-state power generation and in the dynamic frequency response of the diesel generator in a hybrid power system. In steady-state operation the electrical power output of the DEG is a function of the fuel mass flow rate and the total system efficiency which is a combination of combustion, mechanical and generator efficiencies. The fuel input is converted into the electrical power through this efficiency block to produce the steady state power output based on the lower heating value of the fuel.

In the case of dynamic operation, the DEG reacts to both system frequency deviations at the normal operating frequency of the plant, which are induced by load changes. This response is modelled with a governor engine transfer function done with droop control and integral action on the steady state frequency error. The dynamics of the governor is modeled by a first-order

transfer function having time constant $\boldsymbol{T_g}$ and the dynamics of diesel engine torque is modeled by other first-order block with gain $\boldsymbol{K_e}$ and time constant $\boldsymbol{T_e}$. Together, these blocks represent the processing of a frequency deviation signal via the control and mechanical stages to result in a change to the power output of the generator. This DEG model can accurately represent the fuel and power conversion and the dynamic behavior of meeting load frequency control, which can be used in the stability and performance analysis of hybrid power systems.

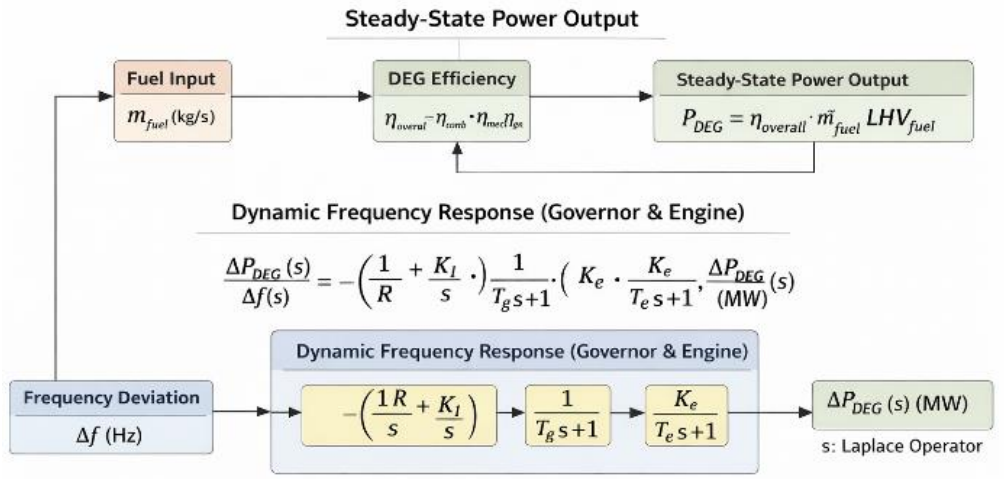


Figure 4. Diesel Engine Generator (DEG) Model for Steady-State Power Output and Frequency Response

The dynamic conversion process of four types of fuel to power supply and the transient frequency control of load frequency response of DEG model are reflected.

3.3.1 Steady-State Power Output

The electrical power output is related to fuel input by:

$$P_{DEG} = \eta_{overall} \cdot \dot{m}_{fuel} \cdot LHV_{fuel} \tag{9}$$

Where:

- $\eta_{overall} = \eta_{comb} \cdot \eta_{mech} \cdot \eta_{gen}$ is the overall conversion efficiency (%),
- $\dot{m}_{fuel}$ is the fuel mass flow rate (kg/s),
- LHV_{fuel} is the lower heating value of the fuel (J/kg).

3.3.2 Dynamic Frequency Response (Governor & Engine)

The variation of DEG power generation (ΔP_{DEG}) with a frequency deviation of the system (Δf) is modeled in the following manner:

$$\frac{\Delta P_{DEG}(s)}{\Delta f(s)} = -\left(\frac{1}{R} + \frac{K_I}{s}\right) \cdot \left(\frac{1}{T_g s+1}\right) \cdot \left(\frac{K_e}{T_e s+1}\right) \tag{10}$$

Where:

- $\frac{1}{R}$ is the droop characteristic (Hz/MW),
- K_I/s represents the integral (reset) control action for zero steady-state error,
- $\frac{1}{T_g s+1}$ models the speed governor dynamics,
- $\frac{K_e}{T_e s+1}$ models the diesel engine torque production dynamics,
- s is the Laplace operator.

3.4 Energy Storage System (ESS) Model

The energy storage system (ESS) model given in Figure 5 explains the dynamic behavior of the stored energy in the hybrid power system and its contribution to power balance and frequency stability in the power system. The battery state of charge (SOC) is the amount of stored energy and is determined by the net amount of power stored over time by taking into consideration the energy capacity of the storage system and the charge/discharge efficiencies of the battery.

During the charging process there is a surplus of power from renewable energy sources increasing the SOC and during discharging there is less energy stored to power the load it's discharged, hence lessening the SOC. This SOC based modeling is used to ensure that the energy availability is tracked realistically and that the storage system does not get overcharged or deeply discharged. In addition, a superconducting magnetic energy storage (SMES) unit is modelled as a fast-acting energy buffer, which is directly responsive to deviations in the system frequency. By injecting/absorbing power quickly in proportion with frequency changes the SMES helps attain immediate frequency support and therefore improve transient stability. Together the battery-based ESS model and SMES model can promote the effective energy management, the power fluctuation smoothing, and improve the entire reliability and dynamic characteristics of the hybrid power system.

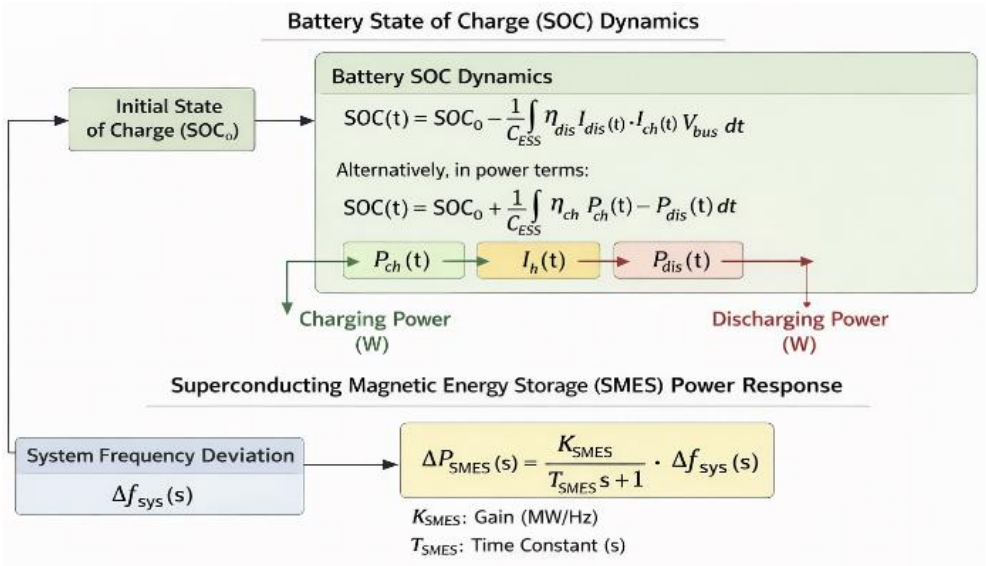


Figure 5. Energy Storage System (ESS) and SMES Model for SOC Dynamics and Frequency Support

3.4.1 Battery State of Charge (SOC) Dynamics

$$SOC(t) = SOC_0 - \frac{1}{C_{ESS}} \int_0^t \left(\eta_{dis} I_{dis}(t) - \frac{I_{ch}(t)}{\eta_{ch}} \right) V_{bus}\, dt \tag{11}$$

Alternatively, in power terms:

$$SOC(t) = SOC_0 + \frac{1}{C_{ESS}} \int_0^t \left(\eta_{ch} P_{ch}(t) - \frac{P_{dis}(t)}{\eta_{dis}} \right) dt \tag{12}$$

Where:

- SOC_0 is the initial state of charge (% or Ah),
- C_{ESS} is the energy capacity (Wh) or charge capacity (Ah),
- η_{ch}, η_{dis} are charging and discharging efficiencies (≤ 1),
- P_{ch}, P_{dis} are charging and discharging powers (W). Sign convention needs to be defined (e.g. charging positive).

3.4.2 Superconducting Magnetic Energy Storage (SMES) Power Response

A reduced form dynamic model for the frequency support is:

$$\Delta P_{SMES}(s) = \left(\frac{K_{SMES}}{T_{SMES} s + 1} \right) \cdot \Delta f_{sys}(s) \tag{13}$$

Where the gain or the amplification is K_{SMES} (MW/Hz) and the time constant is T_{SMES}. The previous Eq. (13) describes an ideal, instantaneous power modulation, based on Converter control, which insofar as system stability is concerned can aptly be described by this, first order transfer function.

3.5 System Integration and Control Theory

3.5.1 Power Balance and Control Error

The basic principle for the real time control is the power balance in the moment:

$$P_{gen}(t) - P_{load}(t) = \frac{dE_{sys}}{dt} \tag{14}$$

For small-signal analysis around an operating point:

$$\Delta P_ctrl\,(t) = \Delta P_load\,(t) - [\Delta P_PV\,(t) + \Delta P_W\,(t) + \Delta P_DEG\,(t) + \Delta P_ESS\,(t)] \tag{15}$$

This clearly defines what ΔP_{ctrl} is, a net power imbalance that is to be compensated from the system inertia and control actions.

3.5.2 System Frequency Dynamics (Swing Equation)

The action of system frequency (f_{sys}) resulting from a power imbalance by the swing equation for single equivalent machine is:

$$2H_{sys} \frac{d\Delta f_{sys}}{dt} = \Delta P_{ctrl}(t) - D\Delta f_{sys}(t) \tag{16}$$

Where:

- H_{sys} is the equivalent inertia constant of the entire HPS (seconds), $J_{sys} = 2H_{sys}S_{base}/\omega_{syn}^2$.
- D is the load damping coefficient (MW/Hz).

3.5.3 System Transfer Function

Taking the Laplace transform of the linearized swing equation (for simplicity we have omitted damping D):

$$\frac{\Delta f_{sys}(s)}{\Delta P_{ctrl}(s)} = \frac{1}{2H_{sys}s} \tag{17}$$

This transfer function is used to build the plant model in order to design the overall system frequency controller. The full block diagram, which would combine the transfer functions of the DEG (governor) as well as the ESS, and of any other controllable sources, would have this inertial response at its core.

3.6 PID Controller Design

A PID controller delivers expanded capabilities beyond a PI controller through its implementation of a derivative term. The system stability improves through error trend prediction which results in better transient response. A PID controller operates through the following mathematical relation:

$$G_c(s) = K_p + \frac{K_i}{s} + K_d s \quad (18)$$

Where:

- The PID controller transfer function is denoted as $G_c(s)$ together with three key elements: K_p and K_i and K_d.
- The proportional gain value K_p responds to current error measurements.
- K_i serves as the integral gain that removes lasting errors from the control system.
- The derivative gain K_d uses future error prediction through rate of change calculation.
- s symbolizes as the Laplace operator.

Three parts of PD regulation control system behaviour: the proportional term for immediate correction, the integral term for steady-state error elimination through past deviation correction, and the derivative term for future error prediction which increases stability and improves transient response.

3.6.1 Objective Function for PID Controller Optimization

The optimization function applies ITSE technology to devise an optimal PID controller that reduces frequency fluctuation. The newly formulated objective function takes this form:

$$J(X) = \int_0^\infty e_f^2(t)dt \quad (19)$$

Where:

- $J(X)$ represents the performance index which needs the minimum value in the design.
- The actual system frequency deviation is shown through $e_f(t)$.

This performance metric applies increasing penalties against larger deviations that occur throughout time which makes the controller operate at its best to minimize frequency disturbances while maintaining system stability.

3.6.2 Sine Cosine Optimized Neural Network Controller for Hybrid System

A sine cosine optimized neural network controller (SCONN) serves to improve system adaptability as part of the system design. The controller enhances its output through dynamic weight adjustment which comes from the utilization of the sine cosine optimization algorithm. The mathematical expression defining an SCONN controller appears as follows:

$$u(t) = W_{out}.f(W_{hidden}.x + b_{hidden}) + b_{out} \quad (20)$$

Where:

- $u(t)$ is the control signal,
- The output weight W_{out} together with the hidden weight W_{hidden} form the model components.
- The input feature vector is designated as x.
- b_{hidden} and b_{out} serve as bias terms when used in the network.
- The activation function $f(.)$ operates during the prediction process (sigmoid or ReLU).

Sine cosine algorithm rules the weight optimization process of the neural network through its iterative weight update procedure of:

$$W^{t+1} = W^{(t)} + r_1.\sin(r_2).\left|W^* - W^{(t)}\right| \quad (21)$$

$$W^{t+1} = W^{(t)} + r_1.\cos(r_2).\left|W^* - W^{(t)}\right| \quad (22)$$

Where:

- The best weight identified thus far corresponds to W^*.
- r_1 and r_2 are random coefficients.

The optimized neural network controller operates as a key control element in the hybrid system because it adapts both frequency and power elements thus enabling better renewable power integration.

3.7 Proposed Controller

The control strategy for the Hybrid Power System integration functions based on controlling error ($\Delta P_{control}$) which determines the difference between changes in load demand (ΔP_{load}) and modifications in net power production (ΔP_{HPS}). The expression for the controlling error takes this form:

$$\Delta P_{control} = \Delta P_{load} - \Delta P_{HPS} \quad (23)$$

Within the framework: the controlling error is $\Delta P_{control}$ *and* ΔP_{load} *indicates load* demand change and ΔP_{HPS} represents net power production modifications.

The controlling error serves as a guide for the control strategy to modify system component power outputs and

enhance system response to demand changes. The description of frequency variation Δf_{HPS} change adopts the following form:

$$\Delta f_{HPS} = \left({}^{1}/_{2\pi}\right) * (\Delta P_{control}/M_{HPS}) \quad (24)$$

The inertia constant of the HPS is represented as M_{HPS}. The system frequency change (Δf_{HPS}) against per-unit power deviation (ΔP_{HPS}) relationship appears in the following transfer function.

$$G_{HPS}(s) = \frac{\Delta P_{HPS}(s)}{\Delta f_{HPS}(s)} = 1/(2\pi * M_{hps} * s) \quad (25)$$

The dynamic relationship between frequency variation and power deviation exists in the Hybrid Power System as represented through its transfer function which supports stable system operation.

Figure 6 shows the Simulink diagram of the microgrid-connected hybrid power system, comprising solar PV, wind (PW), diesel engine generator (DEG), load demand, SMES unit, neural network (NN) controller, PID controller and the swing equation block of the frequency dynamics.

Figure 7 illustrates the architecture of the proffered neural network optimized controller as well as the PI controller, where the input to the network is the error signal, two hidden layers with weighted connections and biases, and the output layer, that produces the compensation signal Vcomp.

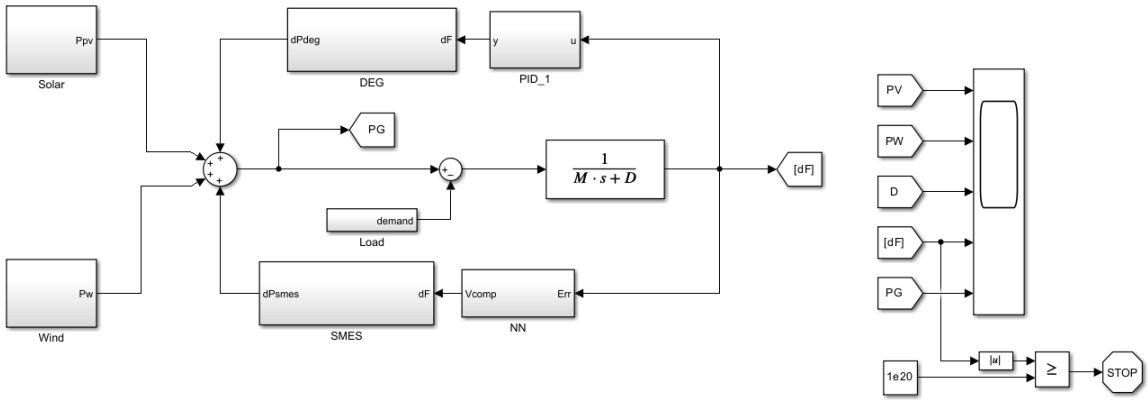


Figure 6. Modeling of Micro-Grid Connected Hybrid Power System

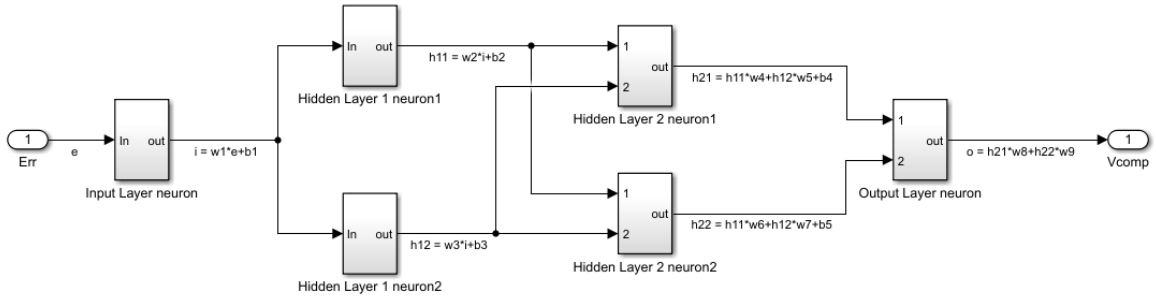


Figure 7. PI and Neural Network-Optimized Controller Design

3.8 Sine Cosine Optimized Neural Network Controller (SCONN) for Optimal Frequency Deviation Compensation

The system adopts a SCONN controller that combines SMES units with PID-controlled diesel generators for optimal frequency regulation purposes. Through its dynamic control functions the SCONN controller enables the SMES system to deliver fast response times by directing power flow in or out depending on frequency fluctuations for demand stability. The DEG possesses a PID controller by which the SCONN algorithm enhances generator response to frequency changes while the PID controller maintains effective secondary frequency regulation. The controller operates weights of the neural network in real-time using the Sine Cosine Optimization (SCO) algorithm to achieve adaptive and precise control outcomes. Combined SMES system frequency correction speed and DEG-PID loop sustained stability lead to exceptional performance in frequency control and system stability against load fluctuations.

3.8.1 Mathematical Model for Sine Cosine Optimized Neural Network (SCONN) Controller in Frequency Regulation

Frequency Deviation Equation: The power system experiences total mismatch during load changes according to the following equation:

$$\Delta P_{mismatch} = \Delta P_{demand} - (\Delta P_{SMES} + \Delta P_{DEG} + \Delta P_{wind} + \Delta P_{PV}) \quad (26)$$

Where:

- The operational mechanism relies on the operation between $\Delta P_{mismatch}$ and ΔP_{demand} to balance power demand and supply.
- Power demand variations during the analysis period should be noted as ΔP_{demand}.
- The power contribution from SMES comes from ΔP_{SMES}.
- The power output capability of the diesel generator stands at ΔP_{DEG}.
- The power supplied by the wind generator is denoted as ΔP_{wind}.
- Energy output from the solar generator is indicated by ΔP_{PV}.

The frequency deviation is determined by swing equation through the following mathematical expression:

$$\Delta f(s) = \frac{\Delta P_{mismatch}}{2\pi J_{sys} s + D} \quad (27)$$

Where:

- J_{sys} is the system inertia,
- D is the damping coefficient,
- s is the Laplace operator.

PID-Controlled Diesel Generator (DEG) Response: This regulation uses a PID controller to control the output power of the diesel generator.

$$G_{PID}(s) = K_p + \frac{K_i}{s} + K_{ds} \quad (28)$$

The diesel generator's frequency deviation response follows:

$$\Delta P_{DEG}(s) = G_{PID}(s).\Delta f(s).\frac{K_{eng}}{\tau_{eng} s + 1} \quad (29)$$

Where:

- K_{eng} is the diesel engine gain,
- τ_{eng} is the diesel engine time constant.

SMES-Based SCONN Controller for Fast Response: The SCONN-based controller operates dynamically to control SMES power injection:

$$\Delta P_{SMES}(s) = G_{SCONN}.\Delta f(s) \quad (30)$$

The optimized neural network controller $G_{SCONN}(s)$ derives from the application of SCO for tuning purposes. The SCONN controller optimizes SMES power control through the following expression:

$$G_{SCONN}(s) = \sum_{i=1}^{N} w_i.\emptyset_i(\Delta f, \dot{\Delta f}, \Delta P_{mismatch} \quad (31)$$

where $\dot{\Delta f}$ is the derivative of frequency deviation, and $\emptyset_i(\cdot)$ represents the tanh activation function used in the hidden layer neurons.

Combined Control Effect for Optimal Frequency Compensation: The complete system response emerges from simultaneous operations of SMES and diesel generator elements.

$$\Delta P_{comp}(s) = \Delta P_{SMES}(s) + \Delta P_{DEG}(s) \quad (32)$$

Substituting (29) and (30) into (32):

$$\Delta P_{comp}(s) = G_{SCONN}(s).\Delta f(s) + G_{PID}(s).\Delta f(s).\frac{K_{eng}}{T_{eng}^{s} + 1} \quad (33)$$

The control goal for optimal frequency compensation aims at reducing frequency deviations:

$$min \int_0^{\infty} \left(\Delta f(t)\right)^2 dt \quad (34)$$

Real-time adaptation through SCO operates by modifying the neural network weights w_i using $G_{SCONN}(s)$ parameters that SCO algorithm optimizes.

3.8.2 Neural Network Architecture and Training Using Sine Cosine Optimization

The proposed Sine Cosine Optimized Neural Network (SCONN) controller is a three-layer feedforward neural network which is composed of three layers that include an input layer, a single hidden layer and output layer.

- ***Input layer:*** It takes three input signals: the frequency deviation of the system Δf , its derivative $\Delta \dot{f}$ and the mismatch in power $\Delta P_{mismatch}$. The min max scaling method is used to normalize all the inputs to the range to $[-1,1]$.
- ***Hidden layer:*** The hidden layer will have 10 neurons transferred by a hyperbolic tangent (tanh) activation function that is useful in aiding topped-off frequency bursts with smooth non-linear fieldwork to non-saturation.
- ***Output layer:*** A single linear neuron generates control signal $u(t)$ which directly adjusts the SMES power injection/absorption.
- ***Training procedure using SCO algorithm:*** The weights of the network (and biases) are optimized by Sine Cosine Optimization (SCO) algorithm as opposed to traditional backpropagation. The SCO algorithm is an algorithm that generates a population of candidate solutions on the set of network parameters (92 parameters: 3×10 input weights + 10 hidden biases + 10×1 output weights + 1 output bias). Under typical load and generation profiles, the maximization is based on the

objective function $J = \int_0^\infty (\Delta f(t))^2 dt$: minimization is carried out over a 100-s simulation horizon.

- ***SCO parameters:*** Population = 30; max iterations = 100; the parameter r_1 (that determines the trade off between exploration and exploitation) is adaptively reduced with iterations: $r_1 = a - t \cdot (a/T_{max})$ where $a = 3$, t is iteration number, $T_{max} = 100$; r_2 is a random number in $[0, 2\pi]$; r_3 and r_4 are random numbers in $[0, 1]$; the trade off between the sine rule and the cosine rule is determined by the rule selectors r_2 and r_3. The equations (21) and (22) indicated above are used to update the weights on the basis of the equations. A maximum number of weights obtained on convergence are saved and used in frequency control online. There is no online retraining done to guarantee deterministic response in real time, but the optimized network yields generalization to unknown disturbances because of the variety of training situations.

4. RESULTS AND DISCUSSION

This section presents the experimental evaluation of the proposed framework as segmentation performance, classification accuracy, comparative evaluation of segmentation and classification performances in different fault conditions. The following Table 1 shows the rating and simulation parameters for the proposed hybrid model.

Table 1. Rating and Parameters of Hybrid Model

Parameter	Value (Rating)
System Power Rating	2 MW (Base)
Capacity of SMES	2 kA
Initial Inductor Current (Ido)	100 kA
Upper Limit of Inductor Current (IdU)	150% of Initial Inductor Current
Lower Limit of Inductor Current (IdL)	30% of Initial Inductor Current
Inertia Constant M	0.12 s
Damping Coefficient D	0.1 MW/Hz
KDEG	1
TDEG	0.5 s
R	0.5
DEG Power	250 KW
Peak PV Power	200 KW
Wind Power	160 KW

Operating Strategy: This section deals with the operating strategy of the considered Hybrid Power System (HPS), for which a SIMULINK diagram is presented in Figure 6. The system/grid frequency is very sensitive to the increase or decrease in load demand. Consequently, any change of load demand is reflected in fluctuations in the system frequency. In order to have a stable and efficient HPS working, grid frequency must be maintained within an acceptable range.

To control the frequency variation, the power supply changes need to follow the changes in the load. When there is a demand for more power, if the grid frequency falls below 50 Hz or has a negative change, the Superconducting Magnetic Energy Storage (SMES) system starts, and it will start to inject power into the grid. Before doing so, however, the SMES unit checks the status of the superconducting coil current (Id) changes with reference to the lower limit of the inductor current (IdL). If Id is greater than IdL, the SMES unit will discharge power into the grid and otherwise standby.

On the other hand, when the grid frequency increases and rises above 50 Hz frequency or positive change occurs in grid frequency, the SMES system absorbs the surplus power by charging the superconducting coil. Before this process takes place, the control unit checks if Id is below the upper limit of the inductor current (IdU). If Id is less than IdU (Id < IdU) then the SMES system continues the charging process else the SMES remains inactive.

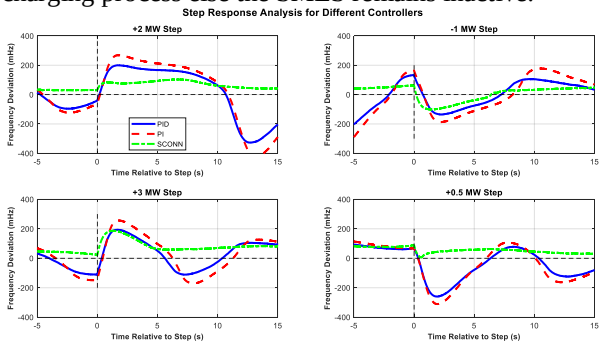


Figure 8. Step Response Comparison of Frequency Deviation for PID, PI, and SCONN Controllers under Load Disturbances

Figure 8 gives step response analysis of system frequency deviation for three different controllers named PID, PI and SCONN considering 4 load disturbance conditions namely +2 MW, -1 MW, +3 MW and +0.5 MW step changes. The frequency deviation is plotted in mHz as a function of time with respect to the step event to observe how each of the controllers responds to sudden imbalance in power. In all cases, the PI controller (red dashed curve) shows the biggest oscillations and higher peak deviations going close to ±300 mHz in some step cases. The PID controller (blue solid curve) is able to reduce the deviation compared with PI but there is still visible overshoot and rather slow settling, particularly for the +2 MW and +0.5 MW disturbances for which the deviation reaches approximately ±200 mHz. The smallest deviation range and smoothness of response and damping is maintained by the SCONN controller (green dotted curve) remaining much closer to the zero-reference line under all step conditions. This comparison shows that the proposed SCONN-based control has a better frequency regulation performance under both positive and negative load variations.

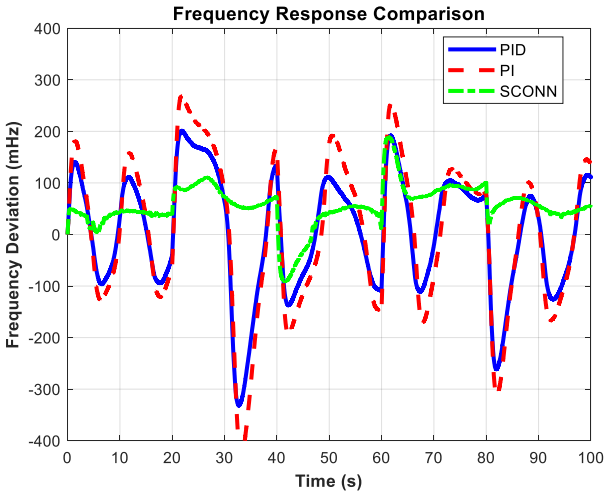


Figure 9. Frequency Deviation Response Comparison of PID, PI, and SCONN Controllers under Dynamic Operating Conditions

Figure 9 gives the frequency response comparison of the hybrid power system using PID, PI, and SCONN controllers with 0-100 s operating interval where frequency deviation is continuously changed with changing load and renewables. The PI controller (red dashed curve) has the largest oscillations with peak deviations becoming close to nearly +250 mHz and nearly -350 mHz which indicates that it has lower damping and sensitivity to disturbances. The PID controller (blue solid curve) offers better regulation than PI, but also has some overshoot and undershoot, which goes to ± 300 mHz at some time instances. The SCONN controller (green dotted curve) remains on a much more level profile, keeping the frequency deviation almost all the time within ±150 mHz and operating faster in terms of dampening after each fluctuation. The response shows the tightness of control provided by the SCONN in terms of frequency stabilization and reduced oscillatory responses for time-varying operating conditions are attained.

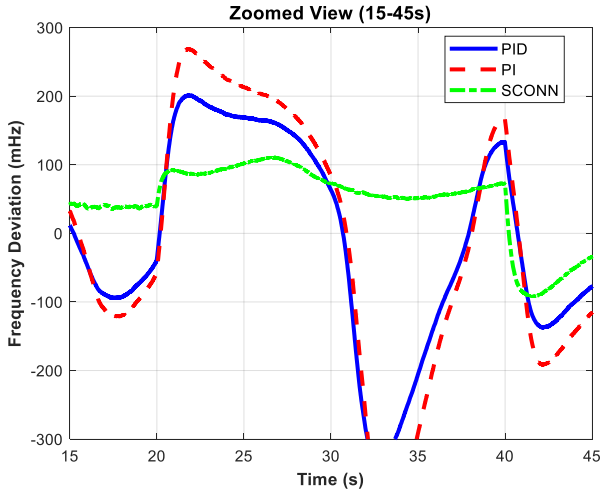


Figure 10. Zoomed Frequency Deviation Response of PID, PI, and SCONN Controllers during 15-45 s Interval

A zoomed view of system frequency deviation response from 15 s to 45 s for PID, PI, and SCONN controllers showing the transient behavior during a disturbance rich operating period is shown in Figure 10. As expected, the PI controller (red dashed curve) has the greatest oscillatory response and deviations of over +250 mHz at about 22 s and deviations of less than -300 mHz at 33-35 s, indicating poor damping and greater overshoot. The PID controller (blue solid curve) better controls the deviation than PI, but still has large excursions, reaching near to +200 mHz at the positive peak of the deviation, and dropping near to -300 mHz during the dip in the negative deviation. The response of the SCONN controller (green dotted curve) is more controlled and the deviations are limited to an area around +120 mHz and minus -100 mHz with a faster recovery of the sharp changes seen near 40 s. The zoomed comparison clearly shows that the SCONN-based controller has a better way of limiting the frequency swings, and a smoother stabilization behavior in the case of rapid system fluctuations.

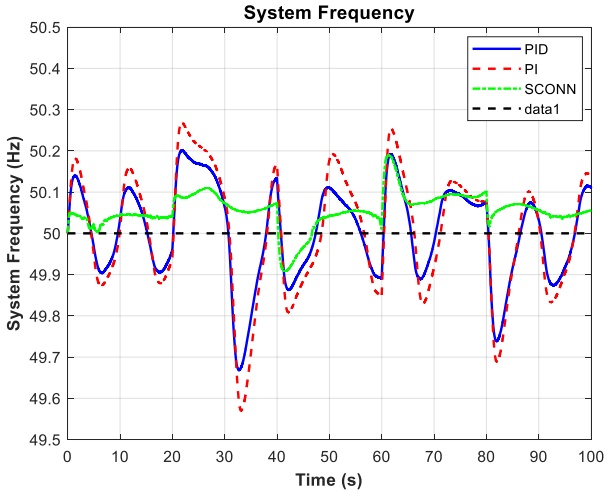


Figure 11. System Frequency Response Comparison of PID, PI, and SCONN Controllers around Nominal 50 Hz

The system frequency response of the hybrid power system under PID, PI and SCONN controllers for a time 0-100 seconds with the nominal reference frequency indicated at 50 Hz as the dashed black line is presented in Figure 11. The PI controller (red dashed curve) exhibits the most significant oscillations of the frequency and peaks of the oscillations approach almost 50.25 Hz and dips close to 49.6 Hz, which means that the regulation is weaker under disturbances. The response of the PID controller (blue solid curve) would be an improvement over PI but still shows during some of the instants quite visible deviations with frequency excursions which occur in a range between 49.7 Hz and 50.2 Hz approximately. The SCONN controller (green dotted curve) achieves the most accurate tracking to the nominal 50 Hz level with smaller fluctuations mostly contained within a narrower band near 49.9 - 50.15 Hz. The plot shows that the SCONN based controller gives

better frequency control and less magnitude of oscillations that support more stable microgrid operation under varying load and renewable generation conditions.

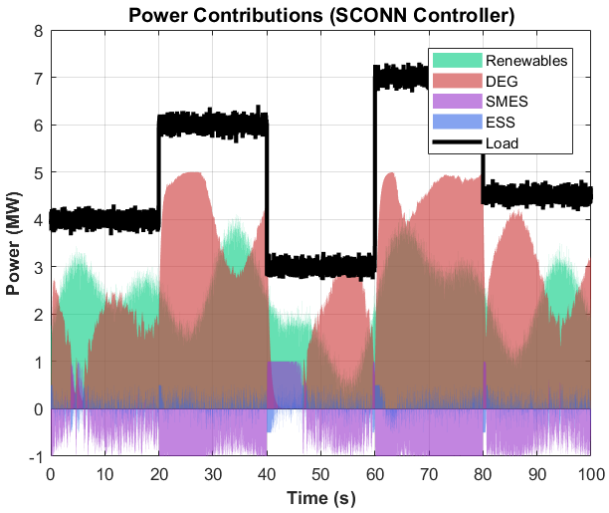


Figure 12. Power Contribution Sharing of Renewables, DEG, ESS, and SMES under SCONN-Based Frequency Control

Figure 12 gives the power contribution profiles of different sources in the hybrid power system under the proposed SCONN controller, on a time interval over the 0-100 s interval, including renewables, diesel engine generator (DEG), energy storage system (ESS), and SMES together with the total load demand which is presented by the black curve. The load changes in a step-wise fashion which goes from nearly 4 MW to about 6 MW around 20s, to almost 3 MW around 40s and back up to more than 7 MW around 60s and finally to around 4.5 MW after 80s. Renewable generation provides generation throughout the year with fluctuating levels during the intervals of higher load demand while DEG ensures the bulk of dispatchable power support during intervals of higher load demand. SMES contribution exhibits quick response in both directions and injects or absorbs power in the order of around ±1 MW at the time of sudden leads response showing the possible role of ready frequency stabilization. The ESS contribution is still quite smaller and smoother comparing to SMES which offers the support to gradual balancing. The plot shows that there should be a coordinated power sharing such that SMES provides the support with fast transient compensation and DEG provides the support for the longer duration power requirements under dynamic working conditions.

Figure 13 shows the comparison of the diesel engine generator (DEG) power output with PID control, PI control and SCONN control operational strategy during the operating duration of 0-100 s. The dynamic changes in DEG power are based on the load changes together with frequency regulation demands, with output from almost 0 MW during off-peak hours up to 5 MW during peak support times. The PI controlled DEG, red dashed curve, there are more and stronger fluctuations, which reflects its worse power regulation. The PID controlled DEG (blue solid curve) gives a better response but there are still noticeable peaks and dips of the response during the rapid transitions, especially around 30-40 seconds and between 80-90 seconds. The control of the SCONN-controlled DEG (green dotted curve) tends to be more controlled - with less oscillatory and attractive adjustments during disturbance periods yet still allowing similar output powers of up to 5 MW when demanded. An important observation from the plot is the smoother DEG power modulation achieved by the SCONN-based approach in which abrupt variations cannot be found and stable frequency control in the hybrid system is supported.

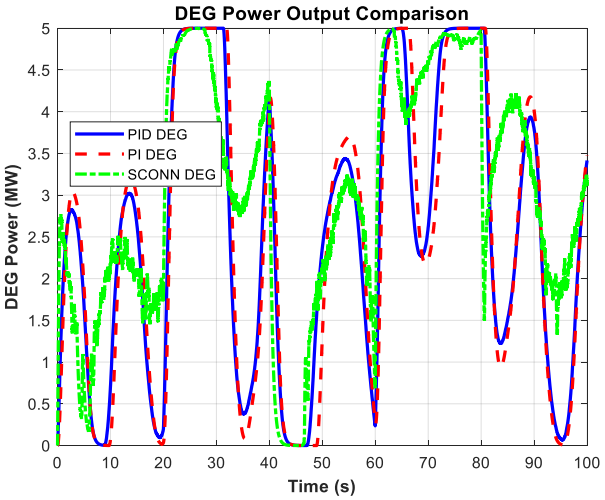


Figure 13. Diesel Engine Generator (DEG) Power Output Comparison under PID, PI, and SCONN Controllers

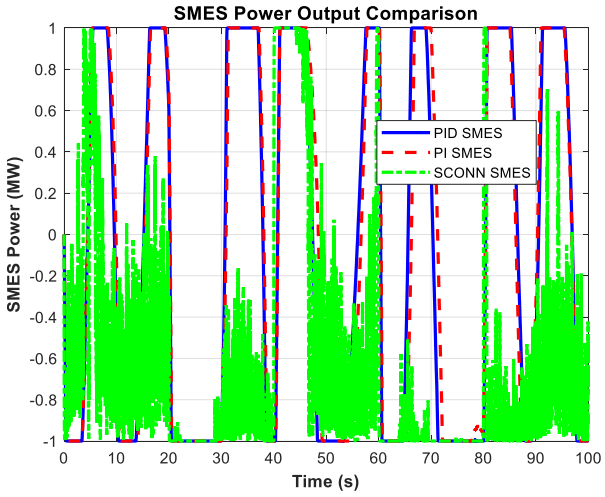


Figure 14. SMES Power Output Comparison under PID, PI, and SCONN Controllers

Figure 14 shows the comparison of the power output of the superconducting magnetic energy storage (SMES) under PID, PI and SCONN control strategies in the 0 - 100 s simulation period. The SMES unit is used as a high-speed frequency support device to feed or absorb power according to frequency deviation in the system, which is

limited to the power output range of about -1 MW to +1 MW. The PID based SMES response (blue solid curve) and PI-based SMES response (red dashed curve) exhibits its frequent switching between maximum charging and discharging limits indicating abrupt control action during disturbance events. The SCONN controlled SMES response - green dotted curve - shows a more adaptive and smoother and more adaptive modulation pattern, for rapid variations within the allowable range, due to its convolution with the role of offering immediate compensation during fluctuations in load and renewable power. The plot shows that the SMES contribution is still limited by the rated capacity; but with SCONN controller, faster adjustment and more flexible power scalability compared to a PID and PI controller for an effective frequency regulation is possible.

Figure 15 shows the comparison of some of the important frequency deviation performance parameters of PID, PI, and SCONN controller such as maximum deviation, RMS deviation, and mean deviation, which is in mHz. The frequency excursion of the PI controller is the largest, the maximum deviation is about 430mHz, the RMS deviation is about 150mHz, and the mean deviation is about 125mHz, so it shows that the control ability of the PI controller is weakest among the three. The behaviour of the PID controller is better than the PI, Max Deviation is approximately 330mHz, RMS Deviation is approximately 115mHz and Mean Deviation is in the 95mHz range.

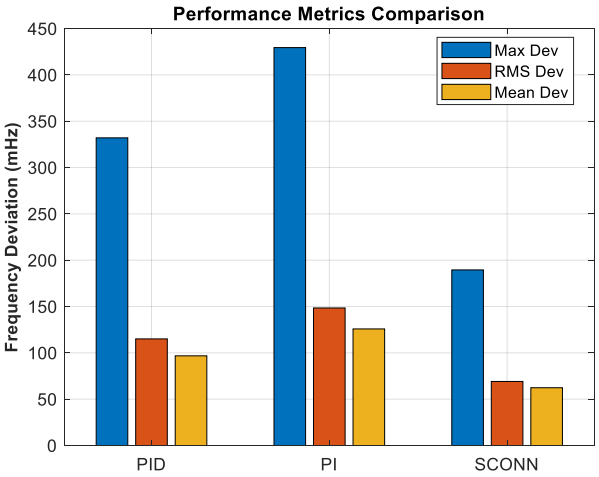


Figure 15. Performance Metrics Comparison of Frequency Deviation for PID, PI, and SCONN Controllers

The SCONN controller, over all metrics, achieves the lowest deviations with the maximum deviation is reduced to about 190 mHz, RMS deviation is about 70 mHz and the mean deviation is about 60 mHz. The bar chart shows that the proposed method of SCONN-based approach ensures a tighter frequency stabilization and also much smaller levels of peak and sustained deviation when compared to conventional PID and PI control methods.

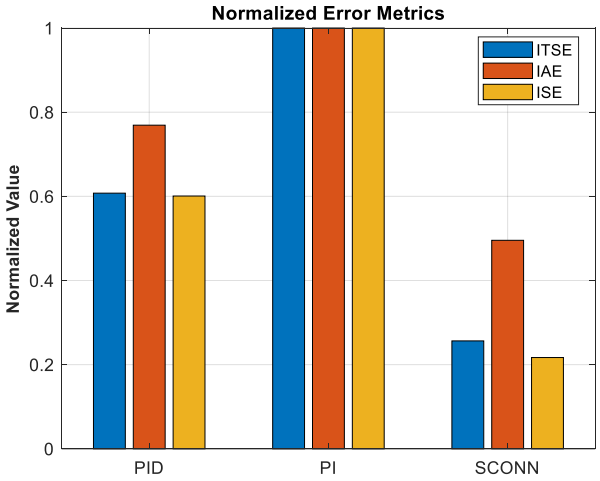


Figure 16. Normalized Error Metric Comparison (ITSE, IAE, and ISE) for PID, PI, and SCONN Controllers

Figure 16 shows the normalized comparison result of three standard frequency control error indices, i.e., ITSE, IAE and ISE of PID, PI and SCONN controller. The PI controller depicts the highest normalized values for all indices that reach the reference value of 1.0 for ITSE, IAE and ISE which signifies the largest accumulated error in the system when it is being operated. The resultant error measures are minimized with normalized ITSE and ISE values near 0.6 and IAE around 0.75 which is less extreme than PI controllers. The lowest error indices are achieved by the SCONN controller with ITSE reduced to almost 0.25 with IAE of around 0.5 and ISE of close to 0.2. The bar chart shows that the proposed SCONN based control strategy provides better results (minimum time and absolute frequency deviation error) than conventional PID and PI controllers.

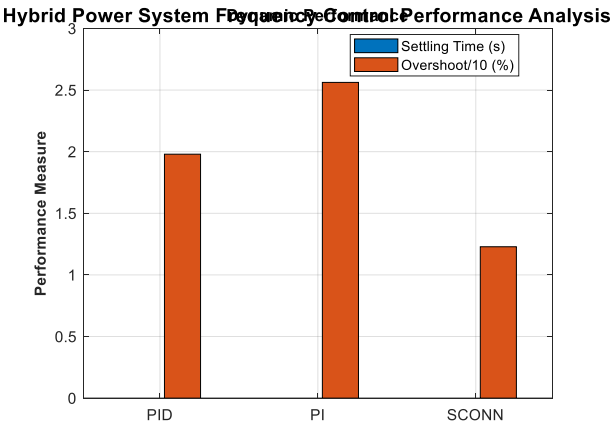


Figure 17. Dynamic Performance Comparison of Settling Time and Overshoot for PID, PI, and SCONN Controllers

Figure 17 is the analysis of dynamic control performance of the hybrid power system with respect to the time of settling, and overshoot for PID, PI and SCONN controller. The Overshoot values are scaled by a factor of 10 for visualization purposes, show that the PI controller generates the significant highest overshoot amount turning up almost 2.6 on the plotted scale, followed by

the PID controller with its overshoot level close to 2.0. The SCONN controller has the lowest overshoot response which is around 1.2, meaning less excursion of transient excitation on frequency disturbances. The comparison shows that the damping characteristics and overshoot limitation of the proposed SCONN-based controller is better than the conventional PI and PID approaches for frequency stabilization, which is helpful to achieve smoother frequency stabilization in the hybrid power system.

Table 2. Performance Comparison between PID and Proposed SCONN Controller

Performance Metric	PID Controller	SCONN Controller	Improvement
Maximum Deviation (Hz)	0.323	0.189	41.4%
RMS Deviation (Hz)	0.115	0.066	42.7%
ITSE	61.658	23.352	62.1%
IAE	9.665	5.870	39.3%
Overshoot (%)	19.9	12.0	39.7% (reduction)

Table 2 shows the performance comparison between the conventional PID controller and the proposed SCONN controller according to the frequency regulation in the hybrid power system. Using the SCONN controller, the maximum frequency deviation is improved from 0.323 Hz to 0.189 Hz with an improvement of 41.4%. The RMS deviation is also reduced from 0.115Hz to 0.066Hz and the ITSE value is also reduced significantly from 61.658 to 23.352. The IAE index is declining from 9.665 to 5.870 which shows that the accumulated frequency error is reduced. Overshoot is lowered from 19.9% to 12.0% having better damping and smoother transient response with the SCONN-based control strategy.

Table 3. Performance Comparison between PI and Proposed SCONN Controller

	PI Controller	SCONN Controller	Improvement
Maximum Deviation (Hz)	0.419	0.189	54.8%
RMS Deviation (Hz)	0.147	0.066	55.5%
ITSE	100.519	23.352	76.8%
IAE	12.514	5.870	53.1%
Overshoot (%)	25.8	12.0	53.3% (reduction)

Table 3 gives the comparative evaluation of conventional PI controller and the proposed SCONN controller at the same operating conditions. The top deviation from 0.419 Hz to 0.189 Hz was limited in the SCONN controller, and is a 54.8% improvement. The RMS deviation is decreased from 0.147 Hz to 0.066 Hz and the ITSE index is majorly reduced from 100.519 to 23.352 which indicates that there is a better dynamic frequency control. The IAE value reduces from 12.514 to 5.870 confirming better Steady performance. Overshoot is reduced from 25.8% to 12.0% showing that the SCONN controller gives better damping and better frequency stabilization than the PI controller.

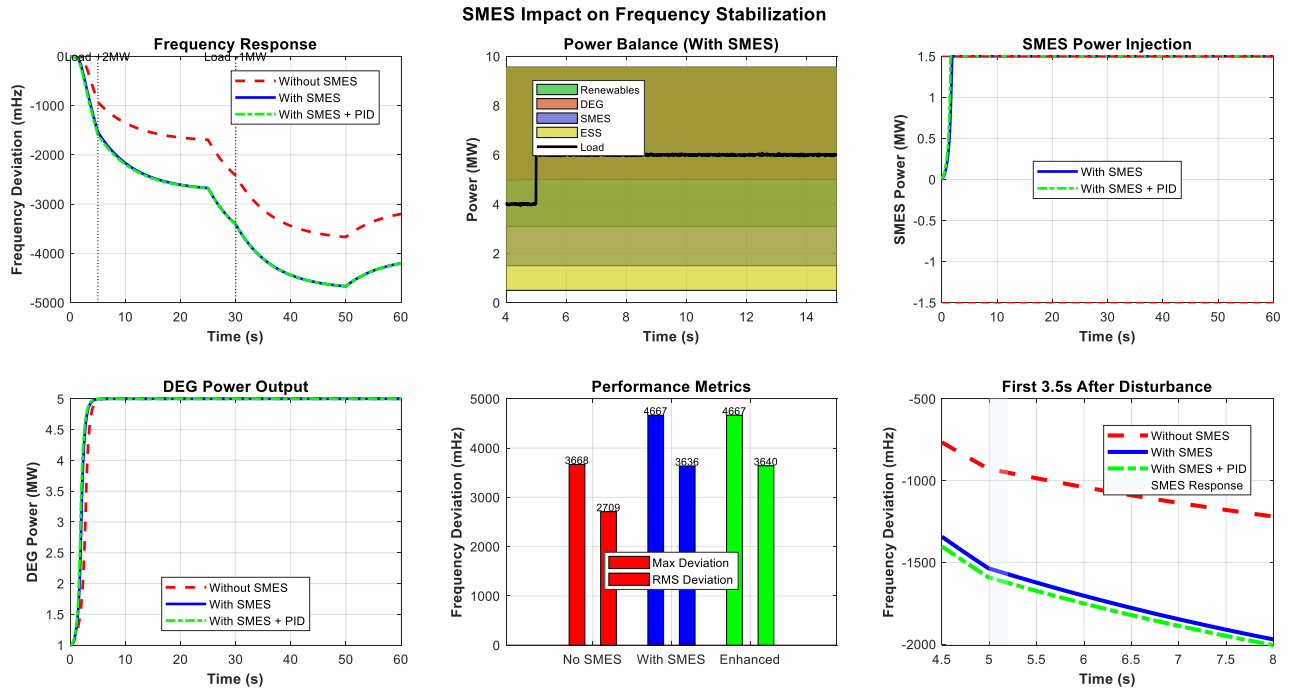


Figure 18. Impact of SMES and Enhanced Control on Frequency Stabilization Performance

Figure 18 shows the effect of integrating SMES and increasing control strategies for frequency stabilization of the hybrid power system by several response plots. The frequency response curve indicates that the case without the SMES has the highest deviation, which is almost -3800 mHz after the disturbance, and the introduction of the SMES can reduce it to about -2700 mHz, and the improved SMES along with PID can make the control response much faster and the recovery faster. The plot of power injection from the SMES shows that the storage unit is fast to immediately provide support after the disturbance, as the power exchange is bounded within around +-1.5MW. The power balance diagram draws attention to concerted contributions of renewables, DEG, SMES and ESS to the fulfillment of load demand. The plot from DEG power outputs indicates that the scale of diesel generation ramps up rapidly towards its rated value around 5 MW in all cases (sustained regulation). A bar chart of performance metrics is presented which compares maximum and RMS Deviation, and the value found through-dev from ~3888mHz (No SMES) to 2790mHz (With SMES) with more improvement under the enhanced control case. The zoomed view of first 3.5 second after disturbance shows that SMES based control delivers an immediate damping and limits the initial frequency drop more well than the system without SMES support.

Table 4. Comparative Results for Various Load Conditions

Load (%)	Controller Type	Efficiency (%)	Total Energy Delivered to Load (J)	Total Energy Supplied by Battery (J)
20	Normal PID	87.34	15683.07965	8346.5206
20	SCONN Optimized PID	88.66	15730.8963	8381.05004
40	Normal PID	87.2	31465.1218	16060.88528
40	SCONN Optimized PID	88.55	31618.2447	16116.77804
60	Normal PID	87.12	47238.6481	24003.60776
60	SCONN Optimized PID	88.6	47411.4214	24131.3424
80	Normal PID	87.1	62976.55805	31945.92544
80	SCONN Optimized PID	88.62	63255.3481	32106.02384
100	Normal PID	87.08	78674.99465	39882.93012
100	SCONN Optimized PID	88.65	79018.1763	40075.2

The results of the evaluation of Normal PID controller performance and SCONN-Optimized PID controller performance under multiple load scenarios for hybrid power system is given in Table 4. The SCONN optimized PID Controller outperformed the Normal PID Controller in all the test periods with improved efficiency and increment of total energy output to the load system and increased energy utilization of battery. The SCONN Optimized PID Controller keeps the efficiency range of 88.55% to 88.66% throughout the processing on the other hand the Normal PID Controller range of 87.08% to 87.34% at always low-level efficiency. The optimized controller generates better load energy transfer than the Normal PID Controller with a continuous increase of energy output till it has its maximum at 79018.1763J at the full load capacity. The optimization of the controller provides for a better energy supply of the battery because it optimizes the power regulation in addition to eliminating more energy losses. The experimental results proved that the SCONN Optimized PID Controller is successful to achieve the superior system stability integrated with the efficiency of the power delivery in microgrid connected hybrid power systems.

Table 5. Comparative evaluation with state-of-the-art methods

Reference	System / Method	Controller & Storage	Max. Freq. Deviation (Hz)	RMS Deviation (Hz)	ITSE	IAE	Overshoot
Saxena & Shankar (2022)	RES-integrated Power System with Hybrid ESS	FOPID + Demand Response; Battery + SC	0.274	0.102	52.418	8.920	14.3%
Safari et al. (2021)	PV + Wind + DEG + EV Microgrid	PSO-ANN Tuned PID; Battery / EVs	0.248	0.094	46.285	7.811	13.8%
Jalilian et al. (2023)	Wind + DEG Hybrid System + SMES	PI/PID + SMES (No Optimization)	0.291	0.109	58.104	9.214	16.5%
Hassan et al. (2024)	PV + Diesel + EV Microgrid	SCO + Balloon Effect Identifier	0.231	0.086	39.775	6.954	12.9%
PI Baseline (Proposed Work)	**PV + Wind + DEG + SMES, 2 MW Microgrid**	**PI Controller + SMES + Battery**	**0.419**	**0.147**	**100.519**	**12.514**	**25.8%**
PID Baseline (Proposed Work)	**PV + Wind + DEG + SMES, 2 MW Microgrid**	**PID Controller + SMES + Battery**	**0.323**	**0.115**	**61.658**	**9.665**	**19.9%**
Proposed SCONN	**PV + Wind + DEG + SMES + Battery, 2 MW Microgrid**	**SCO-Optimized Neural Network + SMES + Battery**	**0.189**	**0.066**	**23.352**	**5.870**	**12.0%**

Table 5 is a comparison of the proposed SCONN controller with the five state-of-the-art methods in literature that have been published recently, and PI and PID baselines. The findings indicate clearly that proposed SCONN has the lowest maximum frequency deviation (0.189 Hz), lowest RMS deviation (0.066 Hz), and lowest ITSE (23.352), IAE (5.870) and overshoot (12.0%), when compared with any other controllers, which support its higher frequency regulation performance.

5. CONCLUSION

This work presented an advanced frequency control framework for microgrid connected hybrid power system combining solar PV, wind generation, diesel engine generator support and superconducting magnetic energy storage unit. The proposed sine cosine optimized neural network controller (SCONN) was designed to control SMES power exchange fast on sudden fluctuations in load and renewable power sources, and the DEG was in-charge of restoring the frequency in a sustained way. Simulation studies under step disturbances and time-varying operating conditions showed that the SCONN strategy demonstrates superior robustness and transient response is better than conventional PI and PID controllers. The maximum deviation of frequency was decreased from 0.323 Hz (PID) and 0.419 Hz (PI) to 0.189 Hz with SCONN control. Error-based indices also improved considerably where ITSE is reduced from 61.658 to 23.352 and overshoot reduced from 19.9% to 12.0%. These results point out the effectiveness of implementing fast response capability with SMES with neural network control optimized using sine cosine algorithm for maintaining stable frequency performance for renewable-rich hybrid microgrids. Future work can include the real-time implementation with experimental validation of the proposed control scheme.

References

Abdolrasol, M. G., Mohamed, R., Hannan, M. A., Al-Shetwi, A. Q., Mansor, M., & Blaabjerg, F. (2021). Artificial neural network based particle swarm optimization for microgrid optimal energy scheduling. *IEEE Transactions on Power Electronics, 36*(11), 12151–12157. https://doi.org/10.1109/TPEL.2021.3074964

Adefarati, T., Bansal, R. C., Shongwe, T., Naidoo, R., Bettayeb, M., & Onaolapo, A. K. (2023). Optimal energy management, technical, economic, social, political and environmental benefit analysis of a grid-connected PV/WT/FC hybrid energy system. *Energy Conversion and Management, 292*, 117390. https://doi.org/10.1016/j.enconman.2023.117390

Adefarati, T., Obikoya, G. D., Sharma, G., Onaolapo, A. K., & Akindeji, K. T. (2024). Design and feasibility analysis of grid-connected hybrid renewable energy system: Perspective of commercial buildings. *Energy Systems, 15*(1), 403–462. https://doi.org/10.1007/s12667-023-00578-z

Babatunde, O. M., Munda, J. L., & Hamam, Y. (2020). A comprehensive state-of-the-art survey on hybrid renewable energy system operations and planning. *IEEE Access, 8*, 75313–75346. https://doi.org/10.1109/ACCESS.2020.2988397

Belboul, Z., Toual, B., Kouzou, A., Mokrani, L., Bensalem, A., Kennel, R., & Abdelrahem, M. (2022). Multiobjective optimization of a hybrid PV/Wind/Battery/Diesel generator system integrated in microgrid: A case study in Djelfa, Algeria. *Energies, 15*(10), 3579. https://doi.org/10.3390/en15103579

Chen, S. Y., & Chang, C. H. (2022). Optimal power flows control for home energy management with renewable energy and energy storage systems. *IEEE Transactions on Energy Conversion, 38*(1), 218–229. https://doi.org/10.1109/TEC.2022.3198883

Choudhury, S. (2022). Review of energy storage system technologies integration to microgrid: Types, control strategies, issues, and future prospects. *Journal of Energy Storage, 48*, 103966. https://doi.org/10.1016/j.est.2022.103966

Coban, H. H., Rehman, A., & Mousa, M. (2022). Load frequency control of microgrid system by battery and pumped-hydro energy storage. *Water, 14*(11), 1818. https://doi.org/10.3390/w14111818

Dawn, S., Ramakrishna, A., Ramesh, M., Das, S. S., Rao, K. D., Islam, M. M., & Ustun, T. S. (2024). Integration of renewable energy in microgrids and smart grids in deregulated power systems: A comparative exploration. *Advanced Energy and Sustainability Research, 5*(10), 2400088. https://doi.org/10.1002/aesr.202400088

Hassan, A. T., Banakhr, F. A., Mahmoud, M. M., Mosaad, M. I., Rashwan, A. F., Mosa, M. R., ... & Mohamed, T. H. (2024). Adaptive load frequency control in microgrids considering PV sources and EVs impacts: Applications of hybrid sine cosine optimizer and balloon effect identifier algorithms. *International Journal of Robotics and Control Systems, 4*(2), 941-957. https://doi.org/10.31763/ijrcs.v4i2.1448

Iweh, D., Gyamfi, S., Tanyi, E., & Effah-Donyina, E. (2021). Distributed generation and renewable energy integration into the grid: Prerequisites, push factors, practical options, issues and merits. *Energies, 14*(17), 5375. https://doi.org/10.3390/en14175375

Jalilian, M., Rastgou, A., Kharrati, S., & Hosseini-Hemati, S. (2023). Frequency stability of hybrid power system in the presence of superconducting magnetic energy storage and uncertainties. *Journal of Operation and Automation in Power Engineering*, *11*(4), 230–239. https://doi.org/10.22098/joape.2023.9829.1686

Khaleel, M., Yusupov, Z., Nassar, Y., El-Khozondar, H. J., Ahmed, A., & Alsharif, A. (2023). Technical challenges and optimization of superconducting magnetic energy storage in electrical power systems. *e-Prime – Advances in Electrical Engineering, Electronics and Energy*, *5*, 100223. https://doi.org/10.1016/j.prime.2023.100223

Rana, M. M., Romlie, M. F., Abdullah, M. F., Uddin, M., & Sarkar, M. R. (2021). A novel peak load shaving algorithm for isolated microgrid using hybrid PV-BESS system. *Energy*, *234*, 121157. https://doi.org/10.1016/j.energy.2021.121157

Safari, A., Babaei, F., & Farrokhifar, M. (2021). A load frequency control using a PSO-based ANN for micro-grids in the presence of electric vehicles. *International Journal of Ambient Energy*, *42*(6), 688–700. https://doi.org/10.1080/01430750.2018.1563811

Sánchez, A., Zhang, Q., Martín, M., & Vega, P. (2022). Towards a new renewable power system using energy storage: An economic and social analysis. *Energy Conversion and Management*, *252*, 115056. https://doi.org/10.1016/j.enconman.2021.115056

Saxena, A., & Shankar, R. (2022). Improved load frequency control considering dynamic demand regulated power system integrating renewable sources and hybrid energy storage system. *Sustainable Energy Technologies and Assessments*, *52*, 102245. https://doi.org/10.1016/j.seta.2022.102245

Ullah, F., Zhang, X., Khan, M., Mastoi, M. S., Munir, H. M., Flah, A., & Said, Y. (2024). A comprehensive review of wind power integration and energy storage technologies for modern grid frequency regulation. *Heliyon*, *10*(9). https://doi.org/10.1016/j.heliyon.2024.e30466

Ullah, Z., Elkadeem, M. R., Kotb, K. M., Taha, I. B., & Wang, S. (2021). Multi-criteria decision-making model for optimal planning of on/off grid hybrid solar, wind, hydro, biomass clean electricity supply. *Renewable Energy*, *179*, 885–910. https://doi.org/10.1016/j.renene.2021.07.063

Venkatesan, K., & Govindarajan, U. (2019). Optimal power flow control of hybrid renewable energy system with energy storage: A WOANN strategy. *Journal of Renewable and Sustainable Energy*, *11*(1). https://doi.org/10.1063/1.5048446

Yadav, V. V., & Saravanan, B. (2023). Multimachine stability improvement with hybrid renewable energy systems using a superconducting magnetic energy storage in power systems. *Journal of Energy Storage*, *57*, 106255. https://doi.org/10.1016/j.est.2022.106255

Zisos, A., Chatzopoulos, D., & Efstratiadis, A. (2024). The concept of spatial reliability across renewable energy systems-An application to decentralized solar PV energy. *Energies*, *17*(23), 5900. https://doi.org/10.3390/en17235900

M. Mujtahid Ansari
Electrical Engineering,
Government College of Engineering,
Jalgaon,
India
mujtahidansari@gmail.com
ORCID 0000-0001-5823-5011

Prashant J. Gaidhane
Instrumentation Engineering,
Government College of Engineering,
Jalgaon,
India
pjgaidhane@gmail.com
ORCID 0000-0003-1802-9103